PERGAMON

International Journal of Solids and Structures 38 (2001) 4631–4655

INTERNATIONAL JOURNAL OF SOLIDS and STRUCTURES

www.elsevier.com/locate/ijsolstr

Interaction of harmonic waves with a periodic array of interface cracks in a multi-layered medium: anti-plane case

Yue-Sheng Wang [a,*], Dietmar Gross [b]

[a] *Institute of Engineering Mechanics, Northern Jiaotong University, Beijing 100044, People's Republic of China*
[b] *Institute of Mechanics, TU Darmstadt, Hochschulstrasse 1, D-64289 Darmstadt, Germany*

Received 20 October 1999; in revised form 8 July 2000

Abstract

The interaction of anti-plane elastic waves with a periodic array of interface cracks in a multi-layered medium is analyzed in this paper. The number of the layers is arbitrary and the cracks may be distributed on any one of the interfaces. Transfer matrix and Fourier series techniques are used to formulate the mixed boundary-value problem in terms of a Hilbert singular integral equation. Numerical solutions are presented for some typical cases: (i) two bonded half-spaces, (ii) a layer bonded to a half-space, (iii) two half-spaces bonded through a layer, (iv) two layers bonded to a half-space. The dependence of the dynamic stress intensity factors (DSIFs) on the frequency of the incident wave, and the influences of geometric configuration, material combination and incident angle are discussed in detail. The results show that the DSIF–frequency curves involve sharp dips and peaks in many cases, i.e. the DSIF drops to a very low value or rises to a very high value in a surprisingly narrow region of frequency. We analyze this phenomenon in detail and find that the rapid change of the DSIF in a quite narrow frequency region is caused by particular modes of Love waves propagating in the elastic layers.

Keywords: Elastic wave; Scattering; Dynamic fracture; Interface crack; Layered medium

1. Introduction

Interaction of elastic waves with interface cracks is a topic which has been received considerable attention due to the increasing use of the composites in engineering. As is well known, interfaces play an important role in composites as well as in bonded materials. Distributed defects such as micro-cracks and debonded zones often occur on the interface as a result of materials processing, manufacturing, bonding methods and in-service conditions. These defects may cause stiffness degradations, and thus influence the integrative properties of the composites. Both the detection of the interface defects and the dynamic failure of the interface are relevant to the interaction of waves with these defects. The defects are generally modeled as interface cracks. The early investigations on this topic were mainly focused on the case of a single

* Corresponding author. Fax: +86-10-6224-5826.
E-mail address: yswang@center.njtu.edu.cn (Y.-S. Wang).

0020-7683/01/$ - see front matter
PII: S0020-7683(00)00280-8

interface crack between two bonded elastic solids (see the references cited in Wang and Gross, 2000). In fact, multiple cracks may be distributed on the interface arbitrarily or periodically. Kundu (1987, 1988) presented the dynamic analysis of two cracks in a layered half-space or in a three-layered plate under anti-plane transient loading. Zhang (1991a,b) obtained the near- and far-field solutions for interaction of SH waves with a periodic array of interface cracks between two bonded half-spaces. He also discussed the dynamic behavior of periodic cracks near and parallel to an interface (Zhang, 1991c). Wang and Gross (2000) developed a universal method to solve SH-wave propagation in a multi-layered medium with arbitrary number of interface cracks. The method makes use of the transfer matrix, Fourier integral transform and singular integral equation techniques. In the present paper, we extend the method to the interaction of SH waves with a periodic array of interface cracks in a multi-layered medium. Instead of Fourier integral transform, the Fourier series technique is employed in this paper because of the periodicity of the problem.

One of the features of wave propagation in a multi-layered medium is the existence of the surface waves propagating in the layers. The cracks scatter the incident waves and produce such surface waves, which makes the problem more complex than in the system of two bonded half-spaces. In this paper, it is shown that some new phenomena arise in wave scattering of periodic cracks in a multi-layered medium due to the surface waves (i.e. Love waves for the present anti-plane case).

Compared with the periodic interface crack problem, the interaction of elastic waves with periodic cracks in homogeneous media has been investigated more early and extensively. Achenbach and his co-workers have made great contributions in this field and presented the far-field solution (see, for instance, Angel and Achenbach, 1985a,b, 1987; Achenbach and Li, 1986; and Mikata and Achenbach, 1988). Zhang (1990, 1992) analyzed the similar problem in both isotropic and transversely isotropic solids, presenting the near-field solution.

2. Problem formulation

The problem considered in this paper is shown in Fig. 1. N layers are bonded to a half-space. All layers and the half-space are homogeneous, isotropic, linearly elastic, with shear modulus μ_r and mass density ρ_r

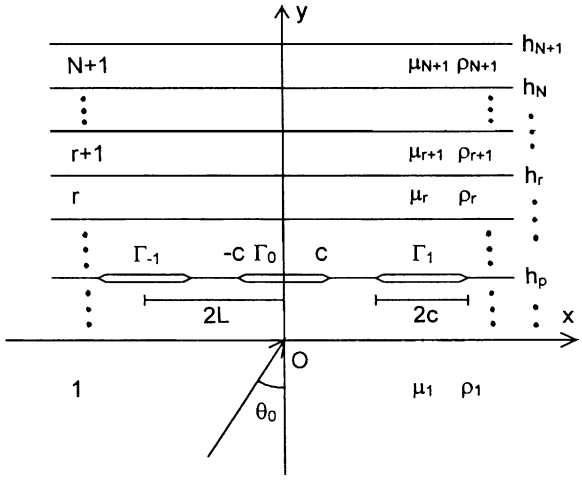

Fig. 1. An array of periodic interface cracks in a multi-layered medium subjected to SH waves.

($r = 1 \ldots N+1$). The shear wave velocity is given by $C_{T_r} = \sqrt{\mu_r/\rho_r}$. The interface between the rth and (r+1)th layer is denoted as the rth interface ($r = 1 \ldots N$). Periodic Griffith cracks of length $2c$ and midpoint distance $2L$ are distributed on the pth interface. Take the x-axis along the surface of the half-space, and the y-axis through the center of a crack. The y-coordinate of the rth interface is denoted as h_r ($h_1 = 0$). The crack occupying the region $|x| \leqslant c$ is represented by Γ_0, and the others at its left and right by $\Gamma_l (l = \pm 1, \pm 2 \ldots)$. Since we consider the propagation of harmonic SH waves with frequency ω in such a multi-layered medium, the only non-zero displacement component is w in z-direction. As a simpler case, we assume the incident wave of the form

$$w^{(\mathrm{i})} = A_0 \exp(\mathrm{i}K_{T_1}(x \sin\theta_0 + y\cos\theta_0) - \mathrm{i}\omega t), \tag{1}$$

where $K_{T_1} = \omega/C_{T_1}$ is the wave number, θ_0, the incident angle, and $\mathrm{i} = \sqrt{-1}$.

We express the total wave fields in the layers as the superposition of the fields without cracks, $\{w^{(0)}, \tau^{(0)}\}$, and those due to the scattering of the cracks $\{w^{(\mathrm{s})}, \tau^{(\mathrm{s})}\}$, i.e.

$$\{w, \tau\} = \{w^{(0)}, \tau^{(0)}\} + \{w^{(\mathrm{s})}, \tau^{(\mathrm{s})}\}, \tag{2}$$

where $\{w^{(0)}, \tau^{(0)}\}$ can be obtained by the classical transfer matrix method or by other methods (see e.g. Kennett, 1983). They have the form of

$$\{f(y), g(y)\} \exp(\mathrm{i}K_{T_1} x \sin\theta_0 - \mathrm{i}\omega t), \tag{3}$$

where $f(y)$ and $g(y)$ are generally the exponential functions of y. The following analysis will be focused on the solution of $\{w^{(\mathrm{s})}, \tau^{(\mathrm{s})}\}$. For convenience, we omit the superscript (s) without confusion and drop the harmonic term $\exp(-\mathrm{i}\omega t)$ throughout the paper.

The Helmholtz equation for SH-wave motion in the rth layer is (Achenbach, 1973)

$$\nabla^2 w_r + K_{T_r}^2 w_r = 0, \quad r = 1 \ldots N+1, \tag{4}$$

where $K_{T_r} = \omega/C_{T_r}$ is the wave number. If we denote the displacement discontinuity on the pth interface (the cracking interface) as Δw, which is equal to the crack opening displacements along the cracks and is zero outside the cracks, the boundary conditions may be written as

$$\{w_r,\ \tau_{yzr}\} \to 0, \quad y \to -\infty,\ \ r = 1, \tag{5}$$

$$\tau_{yzr} = 0, \quad y = h_{N+1},\ \ r = N+1, \tag{6}$$

$$\tau_{yzr} - \tau_{yzr+1} = 0, \quad y = h_r,\ \ r = 1 \ldots N, \tag{7}$$

$$w_r - w_{r+1} = \Delta w \delta_{rp}, \quad y = h_r,\ \ r = 1 \ldots N, \tag{8}$$

$$\tau_{yzp} = \tau_{yzp+1} = -\tau_{yzp}^{(0)} = -\tau_{yzp+1}^{(0)}, \quad x \in \Gamma_l,\ \ \forall l,\ \ y = h_p, \tag{9}$$

where δ_{kp} is the Kronecker symbol. The task of the present paper is to find the solution to the mixed boundary-value problem described by Eqs. (4)–(9).

3. Transfer matrix and dual series equations

The geometry of the system is periodic in x-direction with the period $2L$ and the loading is also periodic in x-direction with the form of Eq. (3). Thus the scattered wave field may be written as the following Fourier series:

$$\{w_r,\ \tau_{yzr}\}^{\mathrm{T}} = \sum_{n=-\infty}^{\infty} \{\bar{w}_r(n,y), \bar{\tau}_{yzr}(n,y)\}^{\mathrm{T}} \exp(-\mathrm{i}n\pi x/L) \exp(\mathrm{i}K_{T_1} x \sin\theta_0). \tag{10}$$

The displacement discontinuity Δw has the similar form. We write it as

$$\Delta w(x) = \Delta W(x) \exp(\mathrm{i}K_{T_1} x \sin\theta_0), \tag{11}$$

where $\Delta W(x)$ is a periodic function with period $2L$ and can be expanded in a Fourier series

$$\Delta W(x) = \sum_{n=-\infty}^{\infty} \Delta\bar{w}(n) \exp(-\mathrm{i}n\pi x/L), \tag{12}$$

where

$$\Delta\bar{w}(n) = \frac{1}{2L} \int_{-c}^{c} \Delta W(u) \exp(\mathrm{i}n\pi u/L)\, \mathrm{d}u. \tag{13}$$

Suppose the opening displacement of the crack Γ_0 is Δw_0, which has the same form as Eq. (11) with $x \in \Gamma_0$. Then, the opening displacement of the crack Γ_l, Δw_l $(l = \pm 1, \pm 2 \ldots)$, may be written as

$$\Delta w_l(x + 2lL) = \Delta W(x + 2lL) \exp(\mathrm{i}K_{T_1}(x + 2lL)\sin\theta_0) = \Delta w_0(x) \exp(2\mathrm{i}lLK_{T_1} \sin\theta_0), \quad x \in \Gamma_0. \tag{14}$$

In fact, this is exactly the deduction of Bloch-theory (Bloch, 1928) for wave propagation in a periodic medium (cf. Zhang, 1991a,b). This means that we can solve the problem in one representative period, say, $|x| \leqslant L$.

Substitution of Eq. (10) into Eq. (4) yields the general solution to $\{\bar{w}_r(n,y),\ \bar{\tau}_{yzr}(n,y)\}^{\mathrm{T}}$ (which is denoted by $\{S_r\}$):

$$\{S_r\} = [T_r(y)]\{C_r\}, \quad r = 1 \ldots N+1, \tag{15}$$

where

$$\{C_r\} = \begin{Bmatrix} C_{1r} \\ C_{2r} \end{Bmatrix}, \qquad [T_r(y)] = \begin{bmatrix} \mathrm{e}^{-\beta_r y} & \mathrm{e}^{\beta_r y} \\ -\mu_r\beta_r\mathrm{e}^{-\beta_r y} & \mu_r\beta_r\mathrm{e}^{\beta_r y} \end{bmatrix},$$

with

$$\beta_r = \begin{cases} [s^2 - K_{T_r}^2]^{1/2}, & |s| \geqslant K_{T_r} \\ -\mathrm{i}[K_{T_r}^2 - s^2]^{1/2}, & |s| < K_{T_r} \end{cases}, \tag{16}$$

in which $s = n\pi/L - K_{T_1}\sin\theta_0$.

Similarly, substituting Eqs. (10), (11) and (12) into Eqs. (5)–(8), we have

$$\{C_1\} = \{B\}C_{21}, \qquad \{C_{n+1}\} = \{X\}C_{1,N+1}, \tag{17}$$

$$\{S_r\} - \{S_{r+1}\} = \{\Delta S_r\}, \qquad y = h_r, \quad r = 1 \ldots N, \tag{18}$$

where

$$\{B\} = \{0,1\}^{\mathrm{T}}, \qquad \{X\} = \{1,\ \exp(-2\beta_{N+1}h_{N+1})\}^{\mathrm{T}},$$

and

$$\{\Delta S_r\} = \{\Delta\bar{w}\delta_{rp},\ 0\}^{\mathrm{T}}.$$

The above derivations involve the case of $h_{N+1} \to +\infty$. Eq. (10) implies that the scattered wave field consists of infinite number of wave modes, the forms of which are determined by the value of β_r (Eq. (16)).

The wave modes for $|s| > K_{T_r}$ are standing wave modes, and those for $|s| < K_{T_r}$ are propagating wave modes. The equality $|s| = K_{T_r}$ gives a "cut-off frequency" for the nth wave mode (Zhang, 1991a,b).

Eq. (18) is in fact a recurrence relation. By substituting Eq. (15) into this relation and considering Eq. (17), the undetermined coefficient matrix $\{C_r\}$ can be expressed in terms of $\{\Delta S_p\}$:

$$\{C_1\} = [\bar{E}_p]\{\Delta S_p\}, \tag{19}$$

$$\{C_r\} = ([\bar{L}_{rp}] + [\bar{K}_{rp}]H(r-p-1))\{\Delta S_p\}, \quad r = 2 \ldots N+1, \tag{20}$$

where $H(\ )$ is the Heaviside function, and

$$\begin{aligned}
&[\bar{L}_{rp}] = [\bar{W}_r]^{-1}[\bar{E}_p], \qquad [\bar{K}_{rp}] = -[\bar{W}_r]^{-1}[L_p],\\
&[\bar{E}_p] = \{B\}[1,0][\bar{W}]^{-1}[L_p], \qquad [L_p] = [\bar{W}_p][T_p(h_p)]^{-1},\\
&[\bar{W}] = \{B\}[1,0] - [\bar{W}_{N+1}]\{X\}[0,1],\\
&[\bar{W}_r] = [W_2]\ldots[W_r], \quad r > 1, \qquad [\bar{W}_1] = [\mathrm{I}],\\
&[W_{r+1}] = [T_r(h_r)]^{-1}[T_{r+1}(h_r)].
\end{aligned}$$

Substituting Eqs. (19) and (20) into Eq. (15), and then into Eq. (10), we obtain

$$\{w_r,\ \tau_{yzr}\}^{\mathrm{T}} = \sum_{n=-\infty}^{\infty} [M_{rp}]\{\Delta S_p\} \exp(-\mathrm{i}n\pi x/L) \exp(\mathrm{i}K_{T_1} x \sin\theta_0), \quad r = 1 \ldots N+1, \tag{21}$$

where we have denoted

$$[M_{rp}] = \begin{cases} [T_1(y)][\bar{E}_p], & r = 1,\\ [T_r(y)]([\bar{L}_{rp}] + [\bar{K}_{rp}]H(r-p-1)), & r > 1 \end{cases} \tag{22}$$

which is the transfer matrix of the multi-layered medium with an array of periodic cracks on pth interface. Writing the matrix $[M_{rp}]$ as

$$[M_{rp}] = \begin{bmatrix} * & * \\ m_{rp}(n) & * \end{bmatrix}, \tag{23}$$

we obtain from Eq. (21),

$$\tau_{yzr} = \sum_{n=-\infty}^{\infty} m_{rp}(n)\Delta\bar{w}(n) \exp(-\mathrm{i}n\pi x/L) \exp(\mathrm{i}K_{T_1} x \sin\theta_0), \tag{24}$$

which, when substituted into boundary condition (9) on crack surfaces, yields

$$\sum_{n=-\infty}^{\infty} \hat{m}_p(n)\Delta\bar{w}(n) \exp(-\mathrm{i}n\pi x/L) \exp(\mathrm{i}K_{T_1} x \sin\theta_0) = -\tau_{yz}^{(0)}(x, h_p), \tag{25}$$

in which $\hat{m}_p = m_{rp}|_{y=h_p}$, $x \in \Gamma_l$. The above equation and

$$\Delta w(x) = \sum_{n=-\infty}^{\infty} \Delta\bar{w}(n) \exp(-\mathrm{i}n\pi x/L) \exp(\mathrm{i}K_{T_1} x \sin\theta_0) = 0, \quad x \notin \Gamma_l \tag{26}$$

are dual series equations, which will be transformed to a Hilbert singular integral equation in Section 4.

4. Singular integral equation and numerical solution

We restrict the following analysis to the representative region: $|x| < L$.

Introduce an auxiliary function:

$$\phi(x) = \frac{\partial}{\partial x}[\Delta W(x)], \quad x \in \Gamma_0 \tag{27}$$

or, equivalently,

$$\Delta W(x) = \int_{-c}^{x} \phi(u)\,\mathrm{d}u. \tag{28}$$

Since $\Delta w(c) = \Delta W(c)\exp(\mathrm{i}K_{T_1} c \sin\theta_0) = 0$, therefore

$$\int_{-c}^{c} \phi(u)\,\mathrm{d}u = 0. \tag{29}$$

Substitution of Eq. (28) into Eq. (13) gives

$$\Delta\bar{w}(n) = \frac{1}{2L}\int_{-c}^{c}\left[\int_{-c}^{u}\phi(v)\,\mathrm{d}v\right]\exp(\mathrm{i}n\pi u/L)\,\mathrm{d}u = \begin{cases} -\frac{1}{2L}\int_{-c}^{c} u\phi(u)\,\mathrm{d}u, & n = 0, \\ \frac{\mathrm{i}}{2n\pi}\int_{-c}^{c}\phi(u)\exp(\mathrm{i}n\pi u/L)\,\mathrm{d}u, & n \neq 0 \end{cases} \tag{30}$$

which when substituted into Eq. (25) yields

$$\frac{\mathrm{i}}{2L}\sum_{n=-\infty}^{\infty}\int_{-c}^{c}\hat{M}_p(n)\phi(u)\,\mathrm{e}^{\mathrm{i}n\pi(u-x)/L}\,\mathrm{d}u = -\hat{\tau}_{yz}^{(0)}(x,h_p), \quad x \in \Gamma_0 \tag{31}$$

where

$$\hat{M}_p(n) = \begin{cases} \mathrm{i}u\hat{m}_p(0), & n = 0, \\ (n\pi/L)^{-1}\hat{m}_p(n), & n \neq 0, \end{cases} \tag{32}$$

$$\hat{\tau}_{yz}^{(0)}(x,h_p) = \tau_{yz}^{(0)}(x,h_p)\,\mathrm{e}^{-\mathrm{i}K_{T_1}x\sin\theta_0}. \tag{33}$$

For fixed values of N and p, we can, by using Mathematica (Version 3.0), easily prove that $\hat{M}_p(n)$ has the following asymptotic behavior as $n \to \pm\infty$:

$$\hat{M}_p(n) = \pm\gamma_p + \mathrm{O}(n^{-2}), \quad n \to \pm\infty, \tag{34}$$

where

$$\gamma_p = -\frac{\mu_p\mu_{p+1}}{\mu_p + \mu_{p+1}}. \tag{35}$$

Due to this relation, special care must be taken in interchanging the summation and integration in Eq. (31). However, by considering the relation:

$$\sum_{|n|=1}^{\infty}\mathrm{sgn}(n)\exp(\mathrm{i}n\pi(u-x)/L) = \mathrm{i}\cot\left(\frac{u-x}{2L/\pi}\right), \tag{36}$$

and denoting

$$P_p(u,x) = \frac{\mathrm{i}}{2L}\left\{\hat{M}_p(0) + \sum_{|n|=1}^{\infty}[\hat{M}_p(n) - \mathrm{sgn}(n)\gamma_p]\exp(\mathrm{i}n\pi(u-x)/L)\right\}, \tag{37}$$

Eq. (31) can be converted to a Hilbert integral equation:

$$-\frac{\gamma_p}{2L}\int_{-c}^{c}\phi(u)\cot\left(\frac{u-x}{2L/\pi}\right)\mathrm{d}u+\int_{-c}^{c}\phi(u)P_p(u,x)\,\mathrm{d}u=-\hat{\tau}_{yz}^{(0)}(x,h_p),\quad x\in\Gamma_0. \tag{38}$$

Introducing the substitutions:

$$\begin{cases} x=c\xi, \qquad u=c\eta, \qquad \Phi(\eta)=\phi(c\eta),\\ Q_p(\eta,\xi)=-\frac{1}{\gamma_p}P_p(c\eta,c\xi)+\frac{1}{2L}\cot\frac{c(\eta-\xi)}{2L/\pi}-\frac{1}{\pi c(\eta-\xi)}, \end{cases} \tag{39}$$

we can transform Eq. (38) to a Cauchy singular integral equation:

$$\frac{1}{\pi}\int_{-1}^{1}\frac{\Phi(\eta)}{\eta-\xi}\mathrm{d}\eta+\int_{-1}^{1}c\Phi(\eta)Q_p(\eta,\xi)\,\mathrm{d}\eta=\frac{1}{\gamma_p}\hat{\tau}_{yz}^{(0)}(c\xi,h_p),\quad |\xi|<1 \tag{40}$$

and Eq. (29) to

$$\int_{-1}^{1}\Phi(\eta)\,\mathrm{d}\eta=0. \tag{41}$$

The numerical solution of Eqs. (40) and (41) has been very well developed by Erdogan and Gupta (1972). Set

$$\Phi(\eta)=\frac{F(\eta)}{\sqrt{1-\eta^2}}. \tag{42}$$

Then Eqs. (40) and (41) reduce to

$$\frac{1}{M}\sum_{j=1}^{M}\left[\frac{F(\eta_j)}{\eta_j-\xi_k}+\pi cQ_p(\eta_j,\xi_k)F(\eta_j)\right]=\frac{1}{\gamma_p}\hat{\tau}_{yz}^{(0)}(c\xi_k,h_p), \tag{43}$$

$$\frac{\pi}{M}\sum_{j=1}^{M}F(\eta_j)=0, \tag{44}$$

where $\eta_j=\cos(\pi(2j-1)/2M)$, $\xi_k=\cos(\pi k/M)$, $k=1\ldots M-1$, and M is the number of the discrete points of $F(\eta)$ in $(-1,1)$.

It is worthy of note that the function $\hat{M}_p(t)$ (Eq. (32)), or equally $\hat{m}_p(t)$, may become infinite at some real values of t. We term these points as real poles of $\hat{M}_p(t)$ or $\hat{m}_p(t)$. They correspond to Love waves propagating in the layers. If some of these poles are integer (i.e. the integer poles), the Fredhelm kernel $P_p(u,x)$ in Eq. (38) or $Q_p(\eta,\xi)$ in Eq. (40) will become infinite. Then, the above results cannot be used anymore, and we must derive another set of equations. This will be done in Section 5 with the method similar to that of Angel and Achenbach (1985a,b).

5. Integral equation when $\hat{M}_p$(n) (or $\hat{m}_p$(n)) has integer poles

We assume $\hat{M}_p(n)$ (or $\hat{m}_p(n)$) has an integer pole denoted by n_α. Set

$$\bar{P}_p(u,x)=\frac{\mathrm{i}}{2L}\left\{\hat{M}_p(0)+\sum_{|n|=1}^{\infty}[\hat{M}_p(n)(\delta_{nn_\alpha}-1)-\mathrm{sgn}(n)\gamma_p]\exp(\mathrm{i}n\pi(u-x)/L)\right\}. \tag{45}$$

Then Eq. (38) becomes

$$-\frac{\gamma_p}{2L}\int_{-c}^{c}\phi(u)\cot\left(\frac{u-x}{2L/\pi}\right)\mathrm{d}u+\int_{-c}^{c}\phi(u)\bar{P}_p(u,x)\,\mathrm{d}u+\hat{M}_p(n_\alpha)\times\int_{-c}^{c}\phi(u)\exp(\mathrm{i}n_\alpha\pi u/L)\,\mathrm{d}u\exp(-\mathrm{i}n_\alpha\pi x/L)=-\hat{\tau}_{yz}^{(0)}(x,h_p),\quad x\in\Gamma_0. \tag{46}$$

To obtain the reasonable solution, $\hat{M}_p(n_\alpha)\int_{-c}^{c}\phi(u)\exp(\mathrm{i}n_\alpha\pi u/L)\,\mathrm{d}u$ should be a finite constant which is denoted by b_α. Because $\hat{M}_p(n_\alpha)=\infty$, we must have

$$\int_{-c}^{c}\phi(u)\exp(\mathrm{i}n_\alpha\pi u/L)\,\mathrm{d}u=0. \tag{47}$$

And Eq. (46) may be rewritten as

$$-\frac{\gamma_p}{2L}\int_{-c}^{c}\phi(u)\cot\left(\frac{u-x}{2L/\pi}\right)\mathrm{d}u+\int_{-c}^{c}\phi(u)\bar{P}_p(u,x)\,\mathrm{d}u+b_\alpha\exp(-\mathrm{i}n_\alpha\pi x/L)=-\hat{\tau}_{yz}^{(0)}(x,h_p),\quad x\in\Gamma_0. \tag{48}$$

Eqs. (29), (47) and (48) represent a set of equations for $\phi(u)$ and b_α. The numerical solution follows the same steps as in Section 6. We need to only refer to the equation obtained from Eq. (47):

$$\frac{\pi}{M}\sum_{j=1}^{M}F(\eta_j)\exp(\mathrm{i}n_\alpha\pi c\eta_j/L)=0. \tag{49}$$

Then, Eqs. (43), (44) and (49) yield a linear system of $(M+1)$ equations for the $(M+1)$ complex-valued unknowns $F(\eta_j)$ $(j=1\ldots M)$ and b_α.

Note that $\hat{M}_p(n)$ (or $\hat{m}_p(n)$) may have more than one integer poles for the same frequency. For example, when $\theta_0=0^\circ$, $-n_\alpha$ is also a pole. This case can be dealt with analogously.

6. Dynamic stress intensity factors

Define the dynamic stress intensity factors (DSIFs) for the crack Γ_0 on the pth interface as

$$K_{\mathrm{III}p}^{\pm}=\lim_{x\to\pm c^{\pm}}\left[\sqrt{2|x\mp c|}\tau_{yz}(x,h_p)\right]. \tag{50}$$

The principal part of $\tau_{yz}(x,h_p)$ at the crack tips is

$$\tau_{yz}(x,h_p)=\tau_{yz}(c\xi,h_p)\approx-\frac{\gamma_p}{\pi}\int_{-1}^{1}\frac{\Phi(\eta)}{\eta-\xi}\mathrm{d}\eta\exp(\mathrm{i}K_{T_1}c\xi\sin\theta_0),\quad|\xi|>1. \tag{51}$$

Following the procedure of analysis in Wang and Wang (1996), we get

$$K_{\mathrm{III}p}^{\pm}=-\gamma_p\sqrt{c}F(\pm1)\exp(\pm\mathrm{i}K_{T_1}c\sin\theta_0), \tag{52}$$

by which the numerical results for DSIFs can be obtained. The DSIFs for other cracks can be calculated by using a relation similar to Eq. (14).

7. Numerical examples and discussion

Although the method developed above is quite general, we only present detailed calculation and discussion for some typical examples, including (i) two bonded half-spaces, (ii) a layer bonded to a half-space, (iii) two half-spaces bonded through a layer, and (iv) two layers bonded to a half-space. The interface shearing stresses $\tau_{yz}^{(0)}(x, h_p)$ induced by the incident wave without cracks can be obtained easily and will not be given here. The functions $\hat{m}_p(n)$ for these four examples are given in Appendix A. The calculations are performed with the double-precision complex FORTRAN program. M in Eq. (43) is taken as 40–60. The infinite series in Eq. (37) is replaced by a finite series from -100 to $100 + \mathrm{int}(K_{T_1} L/\pi \sin\theta_0)$. The accuracy of the results can reach 10^{-4} for the considered frequency region ($K_{T_1} c \leqslant 3$). For the higher frequencies, we can take more terms in the finite series to improve the accuracy. All numerical results are carried out by assuming that the mass densities of all materials are identical. The curves of the normalized DSIFs varying with the normalized frequencies ($K_{T_1} c$) are presented, and the influences of the shear modulus, layer thickness, crack distribution and incident angle on the DSIF–frequency relation are examined.

7.1. Example 1: Two bonded half-spaces

Consider an array of periodic cracks lying on the interface between two bonded half-spaces (Fig. 1 with $N = 1$, and $h_2 \to +\infty$). This is the simplest case and has been studied in detail by Zhang (1991a). Here, we would not give more discussion on this example but check our numerical method by comparison with the results of Zhang. The material constants are taken as $\mu_1/\mu_2 = 1.2$ as in Zhang (1991a). Fig. 2 illustrates the DSIF–frequency curves for $\theta_0 = 0°$ with some selected values of L/c. The DSIFs are normalized with respect to $|\tau_0\sqrt{c}|$ (where $\tau_0 = \mu_2 K_{T_2} A_0$) as done by Zhang (1991a), who also gave the same example. One may observe that the present results agree well with those of Zhang except at some special frequencies. For

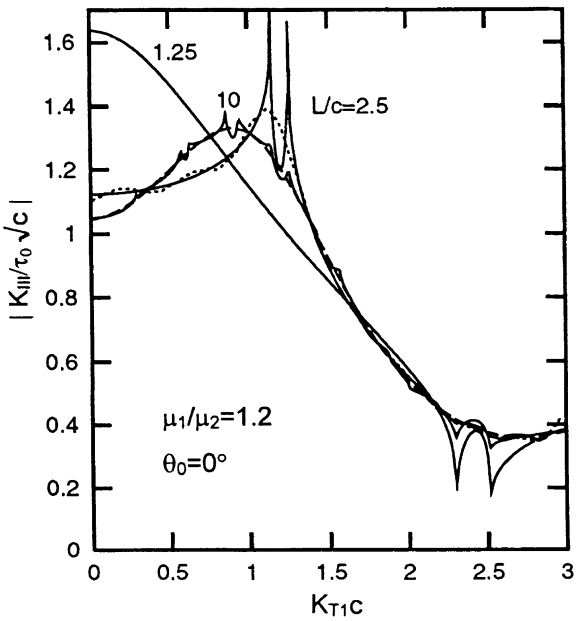

Fig. 2. Normalized DSIF–$K_{T_1} c$ relation with selected values of L/c for two bonded half-spaces. The dashed line is for a single crack, and the dotted line for five cracks.

$L/c = 2.5$, the DSIF has higher and sharper peaks at $K_{T_1}c = 1.1471$ and 1.2566 than that of Zhang, which, we believe, is because we carry out more precise calculation. We calculate DSIFs with increasing $K_{T_1}c$ by 0.0001 near these two particular points. The normalized DSIF reaches 1.74887 at $K_{T_1}c = 1.1471$, and reaches 1.66387 at $K_{T_1}c = 1.2566$. Both are higher than those of Zhang. For the same reason, the DSIF–frequency curve for $L/c = 1.25$ has lower and sharper dips at $K_{T_1}c = 2.2944$ and 2.5134 than that of Zhang. Also for the same reason, the curve for $L/c = 10$ ripples near $K_{T_1}c = 0.3, 0.6, 0.9, 1.2, 1.5, \ldots$, while Zhang's result does not show this character.

We also carry out the computation for the cases of one and five interface cracks using the method we developed before (Wang and Gross, 2000). The DSIF–frequency relation for a single interface crack, demonstrated in the figure by the dashed line, is observed to agree well with that for the periodic cracks with $L/c = 10$ at most frequencies. But no ripples are shown for a single crack. The dotted line shows the DSIF–frequency relation for the middle crack in the case of five interface cracks with $L/c = 2.5$. It agrees with the result for the periodic cracks with $L/c = 2.5$ except in the frequency regions where peaks and dips occur in the latter case. We argue that the appearance of the sharp peaks and dips is one of the distinguishing features of wave scattering by periodic cracks especially when surface waves (e.g. Love waves in the anti-plane motion) propagate in the media. The later results for other examples will support this conclusion.

As another example, we calculate the DSIFs for $\theta_0 = 45°$ with $L/c = 2.5$, and show the results in Fig. 3. By comparison with the Zhang's results, good agreement can be observed except near $K_{T_1}c = 0.7$ where our curves oscillate.

7.2. Example 2: A layer bonded to a half-space

Consider now a periodic array of interface cracks between a layer of thickness h and a half-space (Fig. 1 with $N = 1$ and $h_2 = h < \infty$). The results are shown in Figs. 4–9, where $|\tau_0\sqrt{c}|$ with $\tau_0 = \mu_1 K_{T_1} A_0$ serves to

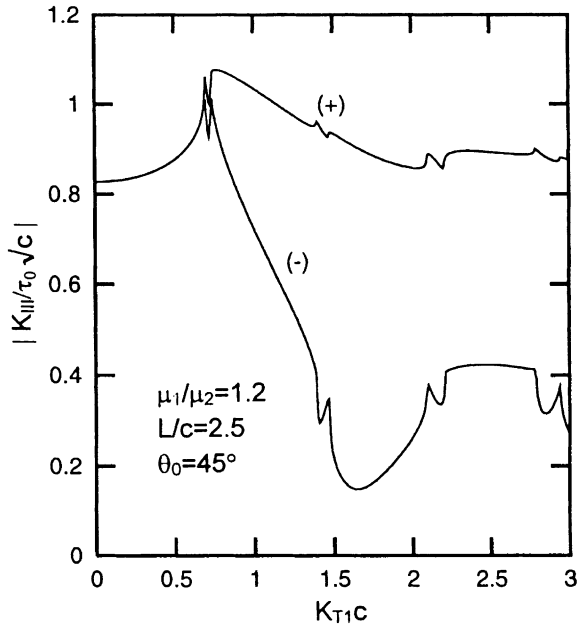

Fig. 3. Normalized DSIF–$K_{T_1}c$ relation with $\theta_0 = 45°$ for two bonded half-spaces.

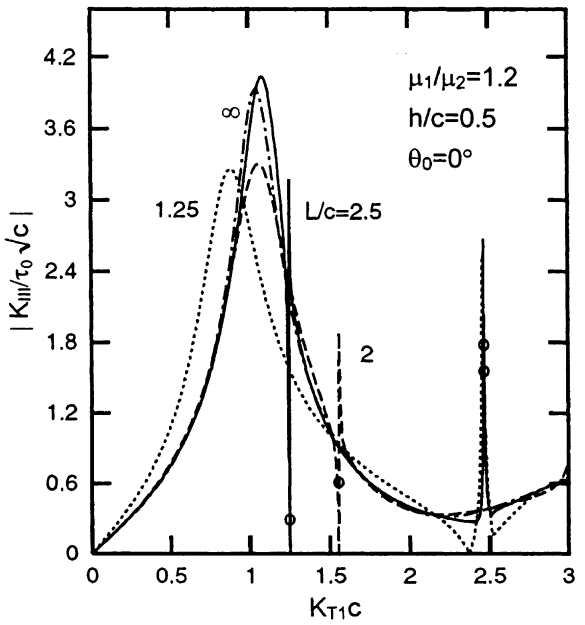

Fig. 4. Effects of crack distribution (L/c) on the normalized DSIF–$K_{T_1}c$ relation for a layered half-space.

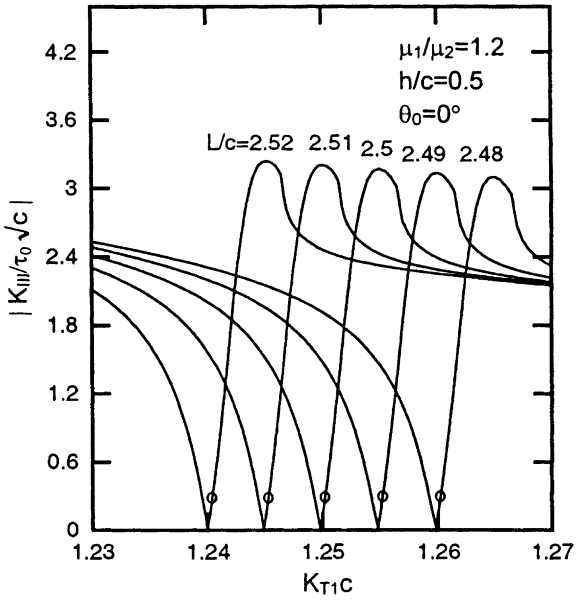

Fig. 5. Effects of crack distribution (L/c) on the normalized DSIF–$K_{T_1}c$ relation in a narrow frequency region for a layered half-space.

normalize the DSIFs. We first examine the effect of the crack distribution (L/c) on the DSIF–frequency relation, which is demonstrated in Fig. 4 for $\mu_1/\mu_2 = 1.2$, $h/c = 0.5$ and $\theta_0 = 0°$ with $L/c = 1.25$ (the dotted line), 2 (the dashed line), 2.5 (the solid line) and ∞ (the case of a single crack, shown by the dot-dashed

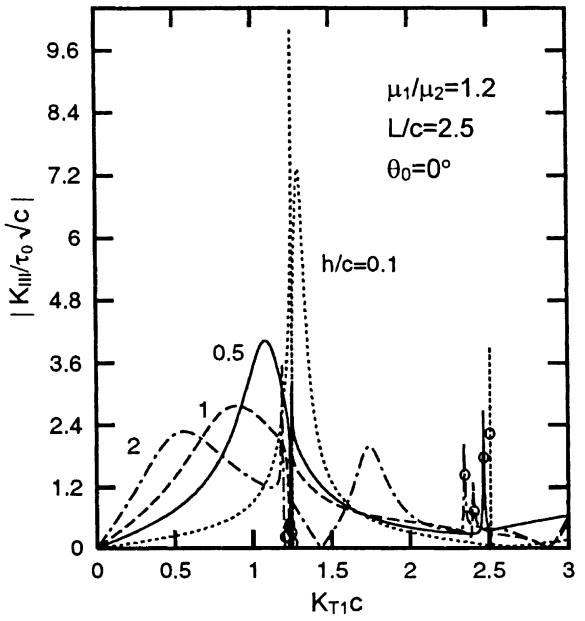

Fig. 6. Effects of layer thickness (h/c) on the normalized DSIF–$K_{T_1}c$ relation a layered half-space.

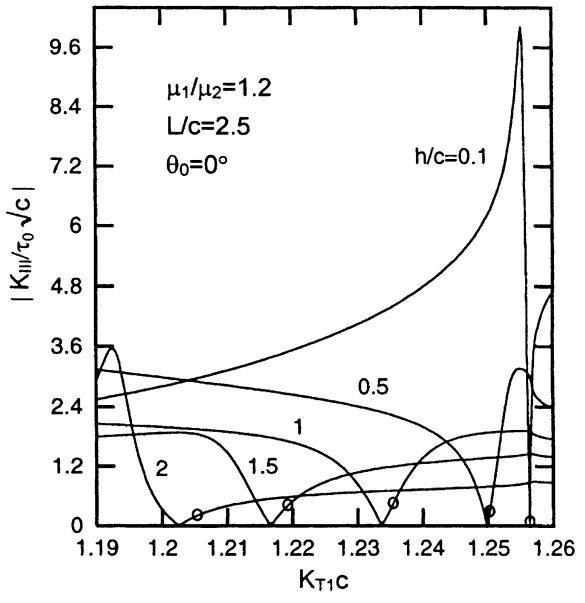

Fig. 7. Effects of layer thickness (h/c) on the normalized DSIF–$K_{T_1}c$ relation in a narrow frequency region for a layered half-space.

line). Besides the resonance peaks between $K_{T_1}c = 0.9$ to 1.1, sharp dips and peaks are observed near $K_{T_1}c = 1.25$ and 2.47 for $L/c = 2.5$, near $K_{T_1}c = 1.55$ for $L/c = 2$, and near $K_{T_1}c = 2.47$ for $L/c = 1.25$. To see clearly the behavior of the DSIF in these special regions, we give a more precise illustration in Fig. 5 for

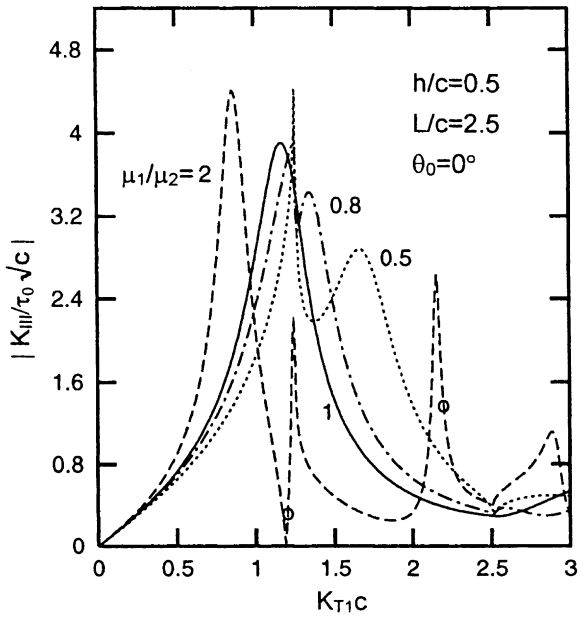

Fig. 8. Effects of material combination (μ_1/μ_2) on the normalized DSIF–$K_{T_1}c$ relation for a layered half-space.

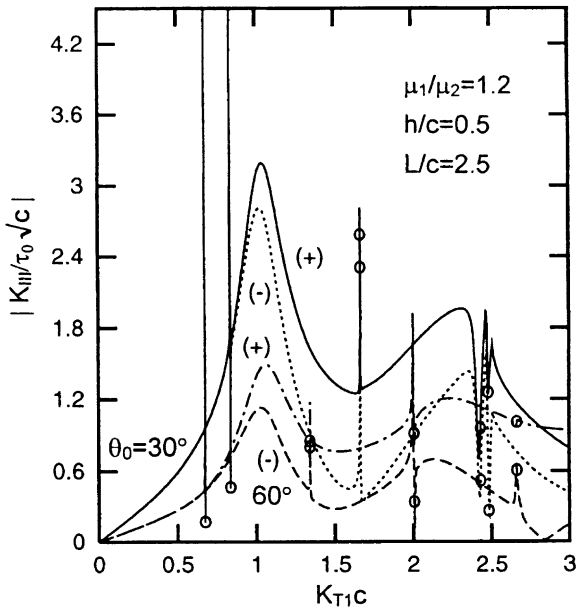

Fig. 9. Effects of incident angle (θ_0) on the normalized DSIF–$K_{T_1}c$ relation for a layered half-space.

the DSIF near $K_{T_1}c = 1.25$ for some selected values of L/c near 2.5. It is shown that the DSIF drops to a very small value (almost to zero) and then rises rapidly to a high value. That is, a dip is followed by a peak. For a bigger value of L/c, the dip appears at a lower frequency.

Table 1
Frequencies and DSIFs when $\hat{M}_p(n)$ has integer poles for a layered half-space with $\mu_1/\mu_2 = 1.2$, $h/c = 0.5$, $\theta_0 = 0°$ and some selected values of L/c

n	$L/c = 2.5$		$L/c = 2$		$L/c = 1.25$	
	$[K_{T_1}c]_L$	$\lvert K_{III}/\tau_0\sqrt{c}\rvert_L$	$[K_{T_1}c]_L$	$\lvert K_{III}/\tau_0\sqrt{c}\rvert_L$	$[K_{T_1}]_L$	$\lvert K_{III}/\tau_0\sqrt{c}\rvert_L$
±1	1.250232	0.28393	1.558759	0.59710	2.470827	1.54488
±2	2.470827	1.76522	3.067966	0.62521	4.821406	0.37444
±3	3.657785	0.31897	4.532076	0.35731	7.115135	0.53308

Why does the DSIF varies so rapidly in such a narrow frequency region? We recall the special case discussed in Section 5 when $\hat{M}_p(n)$ (or $\hat{m}_p(n)$) has integer poles, and find that this case happens exactly in the narrow regions where dips and/or peaks appear. Table 1 lists the frequencies and DSIFs (computed by solving Eqs. (43), (44) and (49)) when $\hat{M}_p(n)$ has integer poles of ±1, ±2 and ±3 for the examples shown in Fig. 4. The corresponding points are depicted in Fig. 4 by circles. Analogous results are also shown in Fig. 5. It is seen clearly that the first dip or peak appears near the frequency at which $\hat{M}_p(n)$ has integer poles of $n = \pm 1$, and the second appears when $n = \pm 2$ are poles, etc. Physically, the dips and peaks occur when certain modes of the Love waves propagate in the layer. However, one may notice that no dips and peaks are observed for a single crack (i.e. $L/c \to \infty$, the dot-dashed line in Fig. 4). This can be explained by the fact that the Love waves generated by the scattering of cracks are dominant in the far field but not near the cracks. Therefore, for a single crack or several concentrated cracks as studied in Wang and Gross (2000), the interaction of Love waves with cracks is negligible. But for periodically distributed cracks, the interaction between Love waves and cracks is important because there are also cracks in the far field. When certain conditions are satisfied, the Love waves will cause rapid change of the DSIF, and therefore sharp peaks and dips appear in the DSIF–frequency curve. By the way, we mention that the resonance peaks appearing between $K_{T_1}c = 0.9$–1.1 (Fig. 4) is due to the interaction of body waves with the cracks as in the case of a single cracks or several concentrated cracks.

The effect of the layer thickness (h/c) on the DSIF–frequency relation is shown in Fig. 6 for $\mu_1/\mu_2 = 1.2$, $L/c = 2.5$ and $\theta_0 = 0°$ with $h/c = 0.1$ (the dotted line), 0.5 (the solid line), 1 (the dashed line) and 2 (the dot-dashed line). The sharp peaks and dips can be observed again for the same reason as we have explained before. As h/c decrease, i.e. the layer becomes thinner with the crack length unchanged, both of the resonance peak induced by the body waves and the sharp peaks and dips induced by Love waves get more pronounced. But the positions of the sharp peaks and dips are not so sensitive to h/c as to L/c. The variation of the DSIF near $K_{T_1}c = 1.25$ is shown more precisely in Fig. 7. The frequencies and the DSIFs are listed in Table 2 and depicted in both two figures by circles for the particular cases when $n = \pm 1$ and ±2 are the poles of $\hat{M}_p(n)$. The results of Figs. 4–7 support the analysis of Section 7.1.

Fig. 8 illustrates the DSIFs versus frequency for different material combinations with $h/c = 0.5$, $L/c = 2.5$ and $\theta_0 = 0°$. The dashed line shows the results for $\mu_1/\mu_2 = 2$, i.e. a low-velocity layer lying on a high-velocity half-space. Sharp dips and peaks appear near $K_{T_1}c = 1.2$ and 2.2. The dotted and dot-dashed

Table 2
Frequencies and DSIFs when $\hat{M}_p(n)$ has integer poles for a layered half-space with $\mu_1/\mu_2 = 1.2$, $L/c = 2.5$, $\theta_0 = 0°$ and some selected values of h/c

n	$h/c = 0.1$		$h/c = 1$		$h/c = 2$	
	$[K_{T_1}c]_L$	$\lvert K_{III}/\tau_0\sqrt{c}\rvert_L$	$[K_{T_1}c]_L$	$\lvert K_{III}/\tau_0\sqrt{c}\rvert_L$	$[K_{T_1}c]_L$	$\lvert K_{III}/\tau_0\sqrt{c}\rvert_L$
±1	1.256363	0.07727	1.235413	0.45180	1.205352	0.20536
±2	2.511096	2.22135	2.410703	0.71966	2.348421	1.42848

lines are, respectively, for $\mu_1/\mu_2 = 0.5$ and 0.8. Both correspond to the case of a high-velocity layer bonded to a low-velocity half-space. Although a sharp resonance peak occurs at $K_{T_1}c = 1.25$, no sharp dips and peaks like in the dashed line are observed. The solid line is for the case of $\mu_1/\mu_2 = 1$, i.e. the semi-infinite homogeneous medium with periodic cracks parallel to the surface. The line is very smooth. No dips and peaks occur. For the reason, we refer to the fact that Love waves do not exist in the last two cases as well known.

Finally, we discuss the effect of the incident angle θ_0. Fig. 9 shows the DSIF–frequency relations for $\theta_0 = 30°$ (solid and dotted lines) and 60° (dot-dashed and dashed lines) with $\mu_1/\mu_2 = 1.2$, $h/c = 0.5$ and $L/c = 2.5$. More dips and peaks are observed for the oblique incidence than for the normal incidence ($\theta_0 = 0°$). The circles in the figure represent the cases when particular modes of Love waves propagate in the layer so that $\hat{M}_p(n)$ becomes infinite. The figure also shows that the incident wave with a small incident angle may cause the larger DSIFs and that the DSIF at the left crack-tip $(-)$ is smaller than that at the right one $(+)$.

7.3. Example 3: Two half-spaces bonded through an interlayer

As the third example, we consider a three layered medium consisting of two half-spaces bonded through an interlayer of thickness h (Fig. 1 with $N = 2$, $h_2 = h$ and $h_3 \to +\infty$). Two interfaces exist in this system, and the periodic cracks may be located on any of them. We first consider the case with cracks on the lower interface (interface 1). Particular attention is focused on the influences of the material combination.

Figs. 10–12 present the results for $\mu_1/\mu_2 = 1$, 0.8 (<1) and 1.2 (>1) respectively, with $h/c = 0.5$, $L/c = 2.5$, $\theta_0 = 0°$ and some selected values of μ_3/μ_2. In the first case (Fig. 10), the cracks are located in the homogeneous half-space and near and parallel to the interface. This is exactly the case studied by Zhang (1991c). The solid line in Fig. 10 shows the result for $\mu_3/\mu_2 = 1.2$ which agrees well with Zhang's result (see Fig. 9 in Zhang, 1991c) except that our curve has more higher and sharper peaks for the same reason as

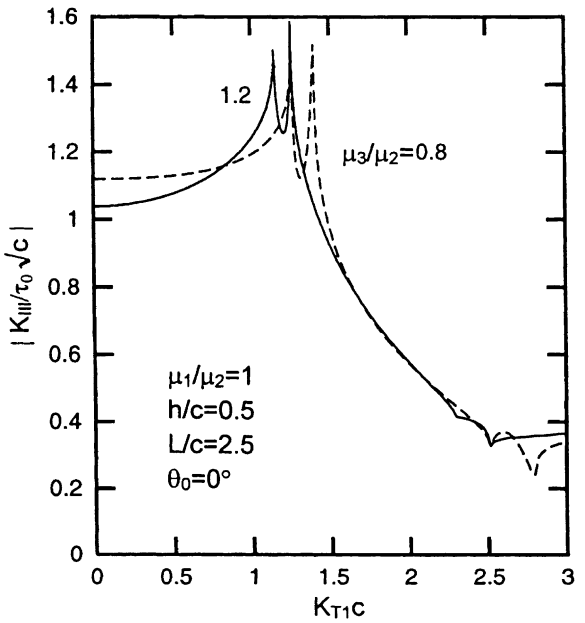

Fig. 10. The normalized DSIF–$K_{T_1}c$ relation for periodic cracks near and parallel to an interface between two half-spaces.

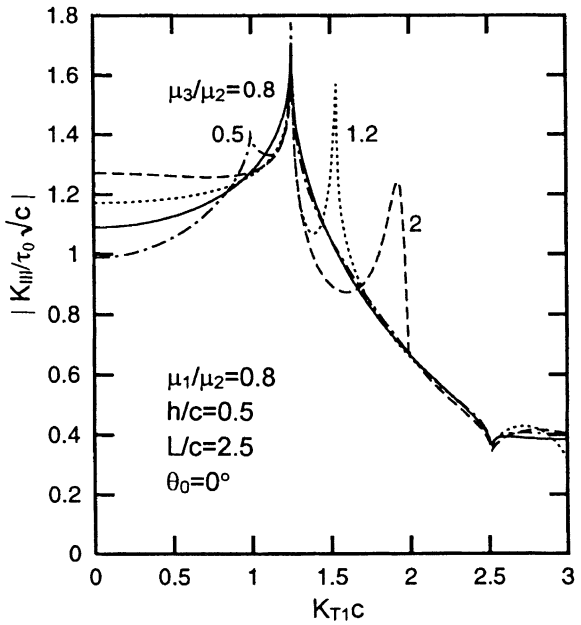

Fig. 11. Effects of material combination (μ_3/μ_2) on the normalized DSIF–$K_{T_1}c$ relation for two half-spaces bonded through a interlayer with periodic cracks on the lower interface, $\mu_1/\mu_2 < 1$.

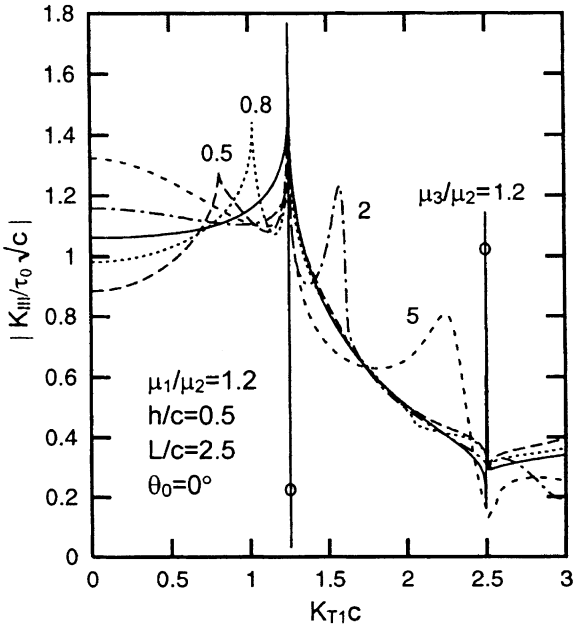

Fig. 12. Effects of material combination (μ_3/μ_2) on the normalized DSIF–$K_{T_1}c$ relation for two half-spaces bonded through an interlayer with periodic cracks on the lower interface, $\mu_1/\mu_2 > 1$.

explained in Section 7.1. The dashed line is for $\mu_3/\mu_2 = 0.8$, that is the lower half-space with cracks is softer than the upper one. It is noted that each curve has double peaks, one of which always appears at $K_{T_1}c = 1.2566$. Another peak appears at the left for $\mu_3/\mu_2 = 1.2$ and at the right for $\mu_3/\mu_2 = 0.8$.

Figs. 11 and 12 show the results for different material combinations. Double peaks are seen for each curves except for $\mu_1{:}\mu_2{:}\mu_3 = 0.8{:}1{:}0.8$ and $\mu_1{:}\mu_2{:}\mu_3 = 1.2{:}1{:}1.2$. As in Fig. 10, every curve has a peak at $K_{T_1}c = 1.2566$. Another peak always appear at the left when $\mu_3/\mu_2 < 1$ and at the right when $\mu_3/\mu_2 > 1$, and it is higher and nearer to the peak at 1.2566 as the value of μ_3/μ_2 approaches 1. A particular case is $\mu_1 = \mu_3$. In this situation, only one peak can be seen. But, it is noted that rapid oscillation of the DSIF, and thus sharp dips and peaks, can be observed at $K_{T_1}c = 1.25$ and 2.50 when $\mu_1 = \mu_3 > \mu_2$ (low-velocity interlayer). This is because that Love waves exist when $\min(C_{T_1}, C_{T_3}) > C_{T_2}$ (Ewing et al., 1957). The circles in the figure show the results when special modes of Love waves occur so that $\hat{M}_p(n)$ becomes infinite. However, we observe no sharp dip and peak for $\mu_1{:}\mu_2{:}\mu_3 = 1.2{:}1{:}2$ and $\mu_1{:}\mu_2{:}\mu_3 = 1.2{:}1{:}5$ (the dot-dashed and dashed lines in Fig. 12) even though Love waves exist in these two cases. This is due to the fact that $\hat{M}_p(n)$ has no integer poles in the frequency region considered here (i.e. $K_{T_1}c = 0$–3). In fact, the first pair integer poles of $\hat{M}_p(n)$ for $\mu_1{:}\mu_2{:}\mu_3 = 1.2{:}1{:}2$ are $n = \pm 5$ at $K_{T_1}c = 6.272627$ which is already beyond the considered frequency region. This is understood by considering that, when the frequency is lower than a certain critical value, Love waves will not exist even in a low-velocity interlayer if the two half-spaces are made of different materials (cf. Eq. (A.8) in Appendix A).

The DSIFs versus frequency are depicted in Fig. 13 for different material combinations with cracks on the upper interface (interface 2). No significant difference is seen between this figure and Figs. 10–12. Therefore, no further results and discussion will be given for this case.

The effects of L/c and h/c are discussed by assuming that the cracks are located on the lower interface. The results are shown in Figs. 14 and 15 for $\mu_1{:}\mu_2{:}\mu_3 = 1.2{:}1{:}1.2$ and $\theta_0 = 0°$. The circles have the same

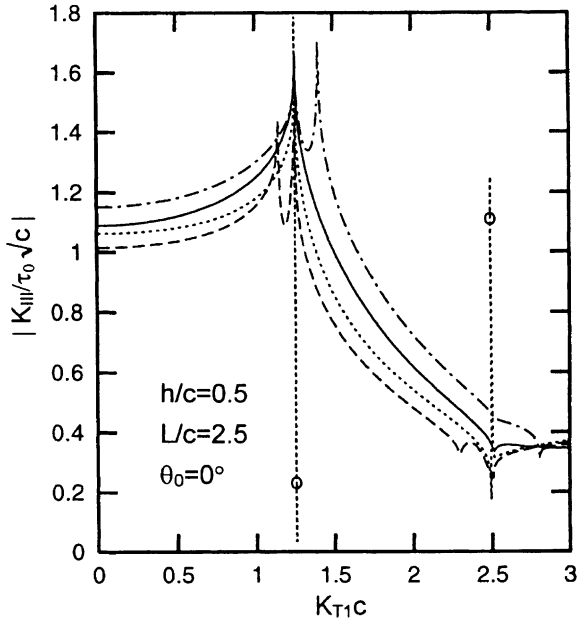

Fig. 13. Effects of material combination ($\mu_1{:}\mu_2{:}\mu_3$) on the normalized DSIF–$K_{T_1}c$ relation for two half-spaces bonded through an interlayer with periodic cracks on the upper interface. (—): 0.8:1:0.8, (- - -): 1.2:1:1, (···): 1.2:1.:1.2, (-·-·-): 0.8:1:1.

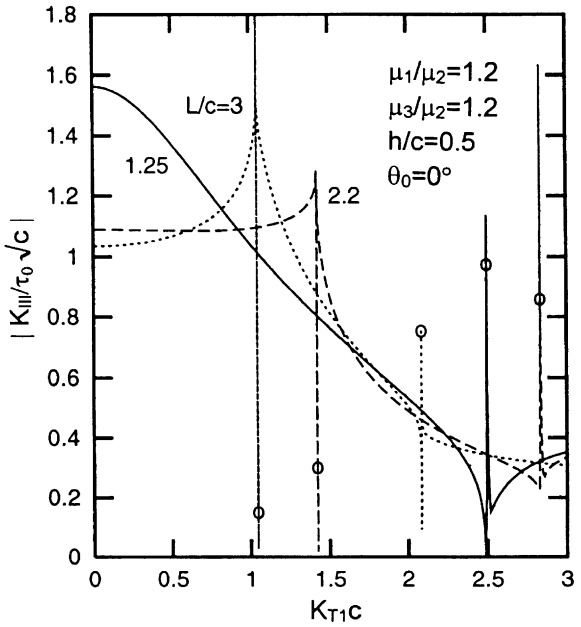

Fig. 14. Effects of crack distribution (L/c) on the normalized DSIF–$K_{T_1}c$ relation for two half-spaces bonded through a layer with periodic cracks on the lower interface.

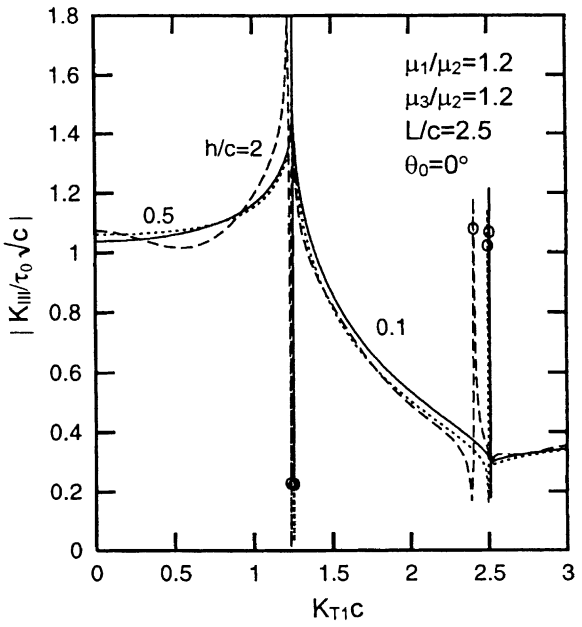

Fig. 15. Effects of layer thickness (h/c) on the normalized DSIF–$K_{T_1}c$ relation for two half-spaces bonded through a layer with periodic cracks on the lower interface.

meaning as before. L/c has obvious influence on the DSIF–frequency relation but h/c does not. It is noted that the dips and peaks are much sharper than those in Section 7.2.

7.4. Example 4: Two layers bonded to a half-space

The last example we consider is a double-layered half-space (Fig. 1 with $N = 2$ and $h_3 < +\infty$). We first calculate the DSIFs for some selected material combinations with $h_3{:}h_2{:}c = 1{:}0.5{:}1$, $L/c = 2.5$ and $\theta_0 = 0°$. The results are shown in Fig. 16 for cracks on the lower interface and in Fig. 17 for cracks on the upper interface. It is noted that sharp dips and peaks occur for $\mu_1{:}\mu_2{:}\mu_3 = 1.2{:}1{:}1.2$ (the solid lines) and $\mu_1{:}\mu_2{:}\mu_3 = 1.2{:}1{:}0.8$ (the dot-dashed lines) but not for $\mu_1{:}\mu_2{:}\mu_3 = 0.8{:}1{:}1.2$ (the dotted lines) and $\mu_1{:}\mu_2{:}\mu_3 = 0.8{:}1{:}0.8$ (the dashed lines). This is easily understood if we recall that condition for the existence of Love waves in a double-layered half-space is $C_{T_1} \geqslant \max(C_{T_2}, C_{T_3})$ (Ewing et al., 1957). The figures also show that the resonance peaks induced by body waves are higher for cracks on the lower interface than on the upper interface. It is worth noting that, in Fig. 18, the solid line has a high peak (reaching 4.6) at $K_{T_1}c = 1.2511$ and that the dot-dashed line has one (reaching 5.6) at $K_{T_1}c = 2.73$.

Next we consider two special situations: one is $\mu_1 = \mu_2$ with cracks on the lower interface, another is $\mu_2 = \mu_3$ with cracks on the upper interface. The first case is indeed a single-layered half-space with cracks in the half-space, and the second is a single-layered half-space with cracks in the layer. In the first case, the x-axis is taken on the upper interface so that $h_2 = 0$ and $h_1 < 0$. The computation is performed for $h_3/c = 1$, $L/c = 2.5$ and $\theta_0 = 0°$. The material combination is chosen as $\mu_1{:}\mu_2{:}\mu_3 = 1.2{:}1.2{:}1$ for the first case and $\mu_1{:}\mu_2{:}\mu_3 = 1.2{:}1{:}1$ for the second case so that Love waves exist and dips and peaks may appear in the DSIF–frequency curves. The influences of the crack position are shown in Fig. 18 for the first case and in Fig. 19 for the second case. The solid line ($h_1/c = 0$) in Fig. 18 is nothing but from the dashed line in Fig. 6 for cracks on the interface. At the lower frequencies, the closer the cracks are to the interface, the higher is the DSIF. But it is contrary at the higher frequencies. Particularly, the dips and peaks caused by special modes

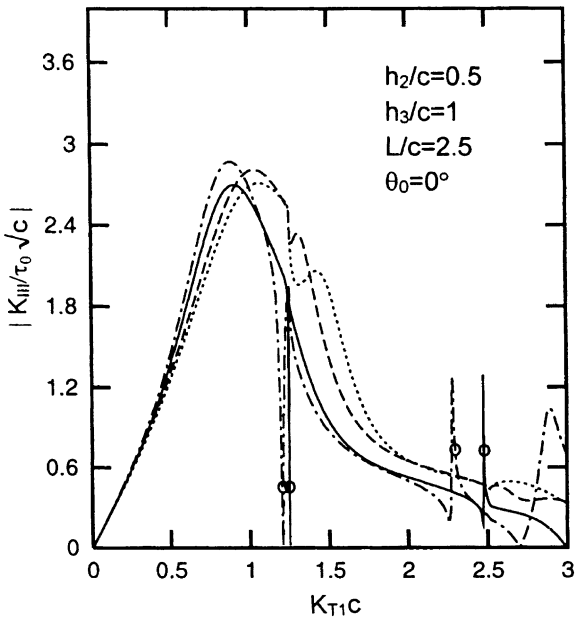

Fig. 16. Effects of material combination ($\mu_1{:}\mu_2{:}\mu_3$) on the normalized DSIF–$K_{T_1}c$ relation for the case of a double-layered half-space with periodic cracks in the lower interface. (—): 1.2:1:1.2, (- - -): 0.8:1:0.8, (· · ·): 0.8:1:1.2, (-·-·-): 1.2:1:0.8.

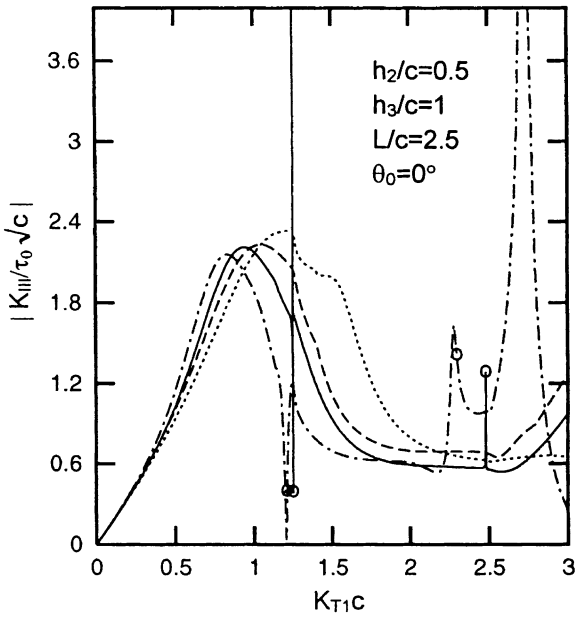

Fig. 17. Effects of material combination (μ_1:μ_2:μ_3) on the normalized DSIF–$K_{T_1}c$ relation for a double-layered half-space with periodic cracks in the upper interface. (—): 1.2:1:1.2, (- - -): 0.8:1:0.8, (· · ·): 0.8:1:1.2, (-·-·-): 1.2:1:0.8.

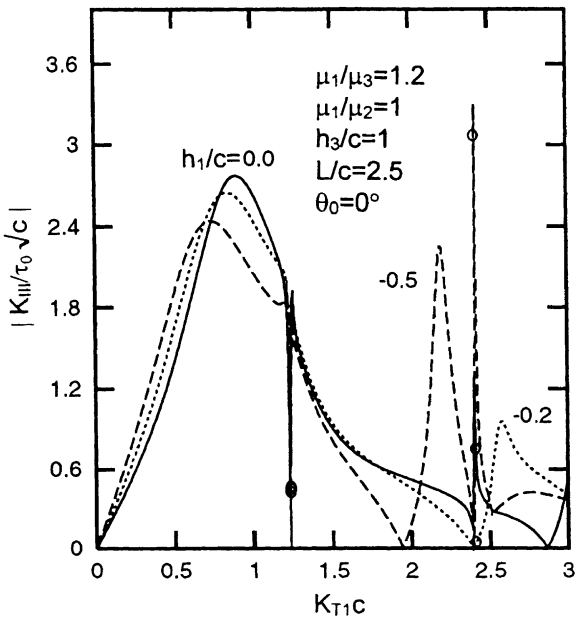

Fig. 18. Effects of crack position (h_1/c) on the normalized DSIF–$K_{T_1}c$ relation for a layered half-space with periodic cracks in the half-space.

of Love waves are more pronounced for cracks far from the interface, and it is noted that the sharp peaks at the higher frequencies are more pronounced (but $h_1/c = -0.2$ is an exception). When the crack array is far

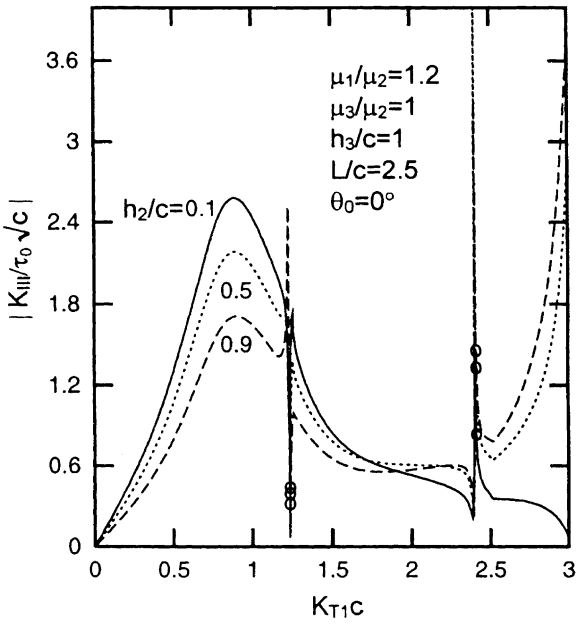

Fig. 19. Effects of crack position (h_2/c) on the normalized DSIF–$K_{T_1}c$ relation for a layered half-space with periodic cracks in the layer.

from the interface, the second resonance peak caused by the body waves at the higher frequencies is more pronounced, especially for the case with cracks in the layer. But the first resonance peak caused by the body waves at the lower frequencies is highest for the interface cracks.

The effect of the layer thickness is examined by assuming that the cracks are along the center of the layer (i.e. $h_3/h_2 = 2$), see Fig. 20. For a thinner layer, the peak near $K_{T_1} = 2.5$ is higher than that near 1.25. But there may be a very high and sharp peak near 1.25 for a thicker layer (see the solid line for $h_3/c = 0.5$). As in the former examples, the layer thickness has no significant influence on the position of the dips and peaks. Fig. 21 presents results for some selected values of L/c to show the effect of the crack distribution. It is found that L/c has the similar effect as in Section 7.2 and 7.3. Here, we find again that the peaks at the higher frequency are more pronounced.

8. Concluding remarks

In the present paper, we develop a general solution for the problem of the interaction of elastic SH-waves with a periodic array of interface cracks in a multi-layered medium. Detailed computation and discussion are presented for some typical examples with emphasis on the sharp dips and peaks appearing in the DSIF–frequency curves in a very narrow frequency region. The analysis shows that these dips and peaks are relevant to the Love waves propagating in the layers. In other words, some particular modes of Love waves may cause rapid change of DSIF in a narrow frequency region. And in some situations, the peak may reach a surprisingly higher level, which, we think, is worthy of notice in practical cases. Generally, we can conclude that Love waves play an important role in the scattering of SH-waves by periodic cracks in layered materials and thus should receive considerable attention.

Finally, we mention that the present method can be extended to the in-plane wave motion which is more significant. The mathematical process is, of course, more cumbersome.

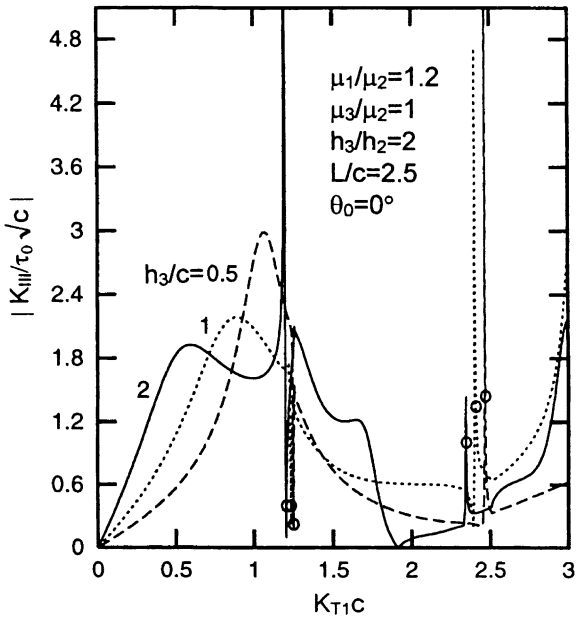

Fig. 20. Effects of layer thickness (h_3/c) on the normalized DSIF–$K_{T_1}c$ relation for a layered half-space with periodic cracks in the layer.

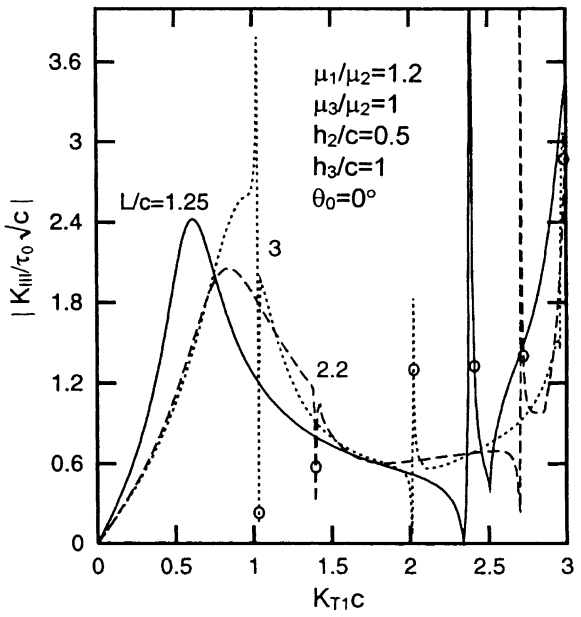

Fig. 21. Effects of crack distribution (L/c) on the normalized DSIF–$K_{T_1}c$ relation for a layered half-space with periodic cracks in the layer.

Acknowledgements

The work was finished during the first author's stay in TU-Darmstadt. Support of the Alexander von Humboldt Foundation is gratefully acknowledged.

Appendix A

The function $\hat{m}_p(n)$ or $\hat{M}_p(n)$ is important in analyzing the behavior of DSIF when Love waves exist. Its integer poles correspond to some particular modes of Love waves which may cause rapid change of DSIF in a very narrow frequency region as we have discussed before. Its detailed expressions for the four examples considered in Section 7 are given in this appendix.

A.1. Example 1: Two bonded half-spaces

$$\hat{m}_1(n) = -\frac{\mu_1\mu_2\beta_1\beta_2}{\mu_1\beta_1 + \mu_2\beta_2}, \tag{A.1}$$

where $\beta_r(n)$ is given by Eq. (16). In this case $\hat{m}_1(n)$ has no real pole.

A.2. Example 2: A layer bonded to a half-space

$$\hat{m}_1(n) = -\mu_1\mu_2\beta_1\beta_2(1 - \mathrm{e}^{-2\beta_2 h})D^{-1}, \tag{A.2}$$

where

$$D = (\mu_1\beta_1 + \mu_2\beta_2) + (\mu_1\beta_1 - \mu_2\beta_2)\mathrm{e}^{-2\beta_2 h}. \tag{A.3}$$

As $h \to +\infty$, (A.2) reduces to (A.1). $D = 0$ yields the well-known Love wave equation in a layered half-space (Love, 1911). It has real roots between K_{T_1} and K_{T_2} when $C_{T_1} > C_{T_2}$. Then, the equation may be written as the typical form

$$\tan|\beta_2|h = \frac{\mu_1\beta_1}{\mu_2|\beta_2|}. \tag{A.4}$$

A.3. Example 3: Two half-spaces bonded through an interlayer

For the cracks on the lower interface (interface 1),

$$\hat{m}_1(n) = -\mu_1\mu_2\beta_1\beta_2[(\mu_3\beta_3 + \mu_2\beta_2) + (\mu_3\beta_3 - \mu_2\beta_2)\mathrm{e}^{-2\beta_2 h}]D^{-1}, \tag{A.5}$$

and for the cracks on the upper interface (interface 2),

$$\hat{m}_2(n) = -\mu_3\mu_2\beta_3\beta_2[(\mu_1\beta_1 + \mu_2\beta_2) + (\mu_1\beta_1 - \mu_2\beta_2)\mathrm{e}^{-2\beta_2 h}]D^{-1}, \tag{A.6}$$

where

$$D = (\mu_1\beta_1 + \mu_2\beta_2)(\mu_3\beta_3 + \mu_2\beta_2) - (\mu_1\beta_1 - \mu_2\beta_2)(\mu_3\beta_3 - \mu_2\beta_2)\mathrm{e}^{-2\beta_2 h}. \tag{A.7}$$

Again $D = 0$ gives the Love wave equation for an interlayer between two half-spaces. Stoneley (1924) investigated this equation and found there are real roots between $\max(K_{T_1}, K_{T_3})$ and K_{T_2} when $C_{T_1}, C_{T_3} > C_{T_2}$. Then, the equation may be written as the typical form

$$\tan|\beta_2|h = \frac{\mu_2|\beta_2|(\mu_1\beta_1 + \mu_3\beta_3)}{\mu_2^2|\beta_2|^2 - \mu_1\mu_3\beta_1\beta_3}. \tag{A.8}$$

It is seen from the above equation that, when the two half-spaces are made of the different materials, there is a certain critical frequency below which the equation has no real root and thus Love waves will not exist.

A.4. Example 4: Two layers bonded to a half-space

For the cracks on the lower interface (interface 1),

$$\hat{m}_1(n) = -\mu_1\mu_2\beta_1\beta_2\big[(\mu_3\beta_3 + \mu_2\beta_2)(1 - e^{-2\beta_3(h_3-h_2)}e^{-2\beta_2h_2}) + (\mu_3\beta_3 - \mu_2\beta_2)(e^{-2\beta_2h_2} - e^{-2\beta_3(h_3-h_2)})\big]D^{-1}, \tag{A.9}$$

and for the cracks on the upper interface (interface 2),

$$\hat{m}_2(n) = -\mu_3\mu_2\beta_3\beta_2\big[(\mu_1\beta_1 + \mu_2\beta_2)(1 - e^{-2\beta_3h_3}) + (\mu_1\beta_1 - \mu_2\beta_2)(1 - e^{-2\beta_3(h_3-h_2)})e^{-2\beta_2h_2}\big]D^{-1}, \tag{A.10}$$

where

$$D = (\mu_1\beta_1 + \mu_2\beta_2)\big[(\mu_3\beta_3 + \mu_2\beta_2) - (\mu_3\beta_3 - \mu_2\beta_2)e^{-2\beta_3(h_3-h_2)}\big] - (\mu_1\beta_1 - \mu_2\beta_2)\big[(\mu_3\beta_3 - \mu_2\beta_2) - (\mu_3\beta_3 + \mu_2\beta_2)e^{-2\beta_3(h_3-h_2)}\big]e^{-2\beta_2h_2}. \tag{A.11}$$

Eqs. (A.5)–(A.7) can be recovered from Eqs. (A.9)–(A.10) by setting $h_3 \to +\infty$. $D = 0$ yields the Love wave equation in a double-layered half-space. Stoneley and Tillotson (1928) and Stoneley (1928, 1950) investigated this equation. They found Love waves exist when $C_{T_1} > C_{T_2}, C_{T_3}$.

The existence and properties of the Love waves in the last three examples considered above are also summarized in the book by Ewing et al. (1957).

References

Achenbach, J.D., 1973. Wave Propagation in Elastic Solids. North Holland, Amsterdam.

Achenbach, J.D., Li, Z.D., 1986. Propagation of horizontally polarized transverse waves in a solid with a periodic distribution of cracks. Wave Motion 8, 371–379.

Angel, Y.C., Achenbach, J.D., 1985a. Reflection and transmission of elastic waves by a periodic array of cracks. Journal of Applied Mechanics 52, 33–41.

Angel, Y.C., Achenbach, J.D., 1985b. Reflection and transmission of elastic waves by a periodic array of cracks: oblique incidence. Wave Motion 7, 375–397.

Angel, Y.C., Achenbach, J.D., 1987. Harmonic waves in an elastic solid containing a doubly periodic array of cracks. Wave Motion 9, 377–385.

Bloch, F., 1928. Über die Quantenmechanik der Elektronen. Z. Physics 52, 555–600.

Erdogan, F., Gupta, G.D., 1972. On the numerical solution of singular integral equations. Quarterly Journal of Applied Mathematics 29, 525–539.

Ewing, W.M., Jardetzky, W.S., Press, F., 1957. Elastic Waves in Layered Media. New York, Mcgraw-Hill.

Kennett, B.L.N., 1983. Seismic Wave Propagation in Stratified Media. Cambridge University Press, Cambridge.

Kundu, T., 1987. Transient response between two interface cracks at the interface of a layered half space. International Journal of Engineering Science 25, 1427–1439.

Kundu, T., 1988. Dynamic interaction between two interface cracks in a three-layered plate. International Journal of Solids and Structures 24, 27–39.

Love, A.E.H., 1911. Some Problems of Geodynamics. Cambridge University Press, London.

Mikata, Y., Achenbach, J.D., 1988. Interaction of harmonic waves with a periodic array of inclined cracks. Wave motion 10, 59–72.

Stoneley, R., 1924. The elastic waves at the surface of separation of two solids. Proceedings of the Royal Society of London Series A 106, 416–428.

Stoneley, R., 1928. Dispersion of waves in a double superficial layer. Monthly Notices of the Royal Astronomical Society, Geophysics, (Suppl 1), 527–531.

Stoneley, R., 1950. The effect of a low-velocity internal stratum on surface elastic waves. Monthly Notices of the Royal Astronomical Society, Geophysics, (Suppl 6), 28–35.

Stoneley, R., Tillotson, E., 1928. The effect of a double surface layer on Love waves. Monthly Notices of the Royal Astronomical Society, Geophysics, (Suppl 1), 521–527.

Wang, Y.S., Gross, D., 2000. Transfer matrix method of wave propagation in a layered medium with multiple interface cracks: anti-plane case. Journal of Applied Mechanics (accepted).

Wang, Y.S., Wang, D., 1996. Scattering of elastic waves by a rigid cylindrical inclusion partially debonded from its surrounding matrix-I. SH case. International Journal of Solids and Structures 33, 2789–2815.

Zhang, Ch., 1990. Interaction of elastic waves with a periodic array of collinear inplane cracks. Acta Mechanica Sinica 8, 328–335.

Zhang, Ch., 1991a. Dynamic stress intensity factors for periodically spaced collinear antiplane shear cracks between dissimilar media. Theoretical and Applied Fracture Mechanics 15, 219–277.

Zhang, Ch., 1991b. Reflection and transmission of SH wave by a periodic array of interface cracks. International Journal of Engineering Science 29, 481–491.

Zhang, Ch., 1991c. Elastodynamic analysis of period antiplane cracks near and parallel to an interface. Engineering Fracture Mechanics 38, 101–110.

Zhang, Ch., 1992. Elastodynamic analysis of a periodic array of mode III cracks in transversely isotropic solids. Journal of Applied Mechanics 59, 366–371.